Monthly Notices of the ROYAL ASTRONOMICAL SOCIETY

MNRAS **463,** 2032–2038 (2016) doi:10.1093/mnras/stw2037
Advance Access publication 2016 August 16

Variability study of the high-mass X-ray binary IGR J18027−2016 with *Swift*-XRT

Nafisa Aftab,[1]★ Nazma Islam[1,2] and Biswajit Paul[1]★

[1]*Raman Research Institute, Sadashivanagar, Bengaluru 560080, Karnataka, India*
[2]*Joint Astronomy Programme, Indian Institute of Science, Bengaluru 560012, Karnataka, India*

Accepted 2016 August 11. Received 2016 August 10; in original form 2015 October 30

ABSTRACT

We report the results from pulsations and spectral analysis of a large number of observations of the high-mass X-ray binary pulsar IGR J18027−2016 with *Swift* X-ray Telescope (XRT), carried out at different orbital phases. In some orbital phases, as seen in different XRT observations, the X-ray intensity is found to vary by a large factor, of about ∼50. In all the observations with sufficient number of source X-ray photons, pulsations have been detected around the previously known pulse period of ∼140 s. When detected, the pulse profiles do not show any significant variation over a flux difference of a factor of ∼3. The absorption column density is found to be large before and after the eclipse. We discuss various possible reasons for intensity and spectral variations in IGR J18027−2016, such as clumpy wind and hydrodynamic instabilities.

Key words: binaries: eclipsing – stars: neutron – X-rays: individual: IGR J18027−2016 – X-rays: stars.

1 INTRODUCTION

High-mass X-ray binary (HMXB) systems contain a companion star with mass $\geq$10 $M_\odot$ (either a main-sequence star or a supergiant) and a compact object (either a neutron star or a black hole). Accretion on to the compact object occurs via capture of stellar wind or Roche lobe overflow. HMXB systems are divided into two classes: (1) Be X-ray binary (Be HMXB) and (2) supergiant X-ray binary (sgHMXB), some of which show the supergiant fast X-ray transient (SFXT) phenomena. Be HMXBs and SFXTs are mostly transients in nature. In Be HMXBs, the accretion on to the compact object occurs via outflowing equatorial disc of the companion star stellar wind and the compact object passing through it (Reig 2011). SFXTs are a sub-class of HMXBs discovered with *INTEGRAL*, having recurrent, bright, short flares (Sguera et al. 2005), reaching $L_X \sim 10^{36}$–10^{37} erg s^{-1} (Sidoli et al. 2007), while their quiescent X-ray luminosity is $\sim 10^{32}$ erg s^{-1} (Bozzo et al. 2010). Persistent sgHMXBs are found to have X-ray luminosity $L_X = 10^{35}$–10^{36} erg s^{-1}, most of the time. Several short off-states have been observed in some of these systems: Vela X-1 – Odaka et al. (2013); Manousakis & Walter (2015), GX 301-2 – Göğüş, Kreykenbohm & Belloni (2011), 4U 1907+09 – Doroshenko et al. (2012), 4U 1700−37 – Grebenev et al. (1999) and OAO 1657−415 – Pradhan et al. (2014). On the other hand, some sgHMXBs like SMC X-1 and LMC X-4 do not show off-states, but they have strong short time-scale flares (Moon & Eikenberry 2001; Moon, Eikenberry & Wasserman 2003). *INTEGRAL* observations of sgHMXBs show a wide range and type of intensity variation (Walter et al. 2015).

The HMXB IGR J18027−2016 was discovered with *INTEGRAL*-IBIS/ISGRI during the survey of the Galactic Centre region in 2003 September (Revnivtsev et al. 2004). The pulsar is found to have a spin period of ∼139 s (Augello et al. 2003) and orbital period of 4.57 d (Hill et al. 2005; Jain, Paul & Dutta 2009) around a supergiant companion with spectral type B1-Ib (Torrejón et al. 2010). Hill et al. (2005) characterized the combined *XMM–Newton* and *INTEGRAL* X-ray spectrum of the pulsar by a broken power law, modified by a photoelectric absorption along the line-of-sight hydrogen column density $N_H \sim 10^{23}$ cm^{-2}. A soft excess is also detected in the spectra of this source (Hill et al. 2005; Walter et al. 2006).

In this work, we have analysed all *Swift*-XRT observations of IGR J18027−2016 to investigate its long-term pulsation and spectral characteristics. We searched for pulsations in all the observations and folded the light curves with the estimated pulse period to study its pulse profiles. Orbital intensity analysis shows some low X-ray intensity episodes of the source, similar to that seen in Vela X-1, GX 301-2, 4U 1907+09 (Göğüş et al. 2011; Doroshenko et al. 2012; Manousakis & Walter 2015) and OAO 1657−415 (Barnstedt et al. 2008). We have further investigated the nature of the system by studying its spectral characteristics at different orbital phases. Our results can put some useful insight into systems having sudden off-states in X-ray intensity.

★E-mail: nafisa@rri.res.in (NA); bpaul@rri.res.in (BP)

Table 1. Log of observations with exposure time, total number of source photons, average count rate, pulse period and orbital phase. A and B refer to the observations which were split as mentioned in Section 2.

Observation MJD	Observation ID	Exposure time (s)	Total no. of photons in source region	Average count rate (counts s^{-1})	Pulse period (s)	Orbital phase
56143	00035720023	929	6	0.01	–	0.02–0.03
56098	00035720011	874	8	0.01	–	0.06–0.08
56085 A	00035720005 A	442	16	0.04	–	0.13
56171	00035720034	2025	22	0.01	–	0.92–0.94
56144	00035720024	2093	26	0.01	–	0.02–0.03
56125	00035720017	2035	29	0.01	–	0.86–0.89
56089	00035720009	989	42	0.04	–	0.25
56157	00035720027	1913	50	0.03	–	0.03–0.05
56156	00035720026	2035	81	0.04	–	0.73–0.75
56167	00035720030	1975	99	0.05	–	0.11–0.13
56170	00035720033	1988	126	0.06	–	0.69–0.70
55751	00035720004	692	127	0.18	–	0.16
54141 B	00035720001 B	3798	142	0.03	–	0.83–0.91
56128	00035720019	1231	180	0.15	–	0.48–0.53
56088	00035720008	2020	204	0.10	–	0.73–0.75
56118	00035720015	1878	218	0.12	–	0.48–0.5
56126	00035720018	1898	252	0.13	–	0.20–0.22
56100	00035720013	2170	282	0.13	–	0.36–0.42
56158	00035720028	1523	376	0.25	–	0.16
56096 B	00035720010 B	327	415	1.18	–	0.63
56099	00035720012	1121	417	0.39	–	0.17–0.23
56096 A	00035720010 A	1059	620	0.56	140.12 ± 0.01	0.58–0.61
56085 B	00035720005 B	852	699	0.73	141.31 ± 0.01	0.28
56113	00035720014	1920	719	0.41	139.69 ± 0.01	0.30–0.31
56155	00035720025	2143	772	0.36	140.01 ± 0.01	0.44–0.45
56124	00035720016	1855	780	0.42	143.35 ± 0.01	0.69–0.72
56086	00035720006	1873	796	0.43	139.75 ± 0.01	0.30–0.31
56159	00035720029	1968	822	0.42	140.01 ± 0.01	0.36–0.39
56140	00035720020	1955	876	0.45	139.66 ± 0.01	0.16–0.17
56168	00035720031	2038	900	0.44	140.14 ± 0.01	0.23–0.25
54531	00035720002	2914	909	0.31	139.66 ± 0.01	0.17–0.23
56142	00035720022	1960	1035	0.53	139.48 ± 0.01	0.69–0.72
56087	00035720007	1446	1329	0.92	143.25 ± 0.01	0.53–0.55
56169	00035720032	1865	1370	0.74	140.20 ± 0.01	0.47–0.48
54141 A	00035720001 A	5789	1617	0.27	139.95 ± 0.01	0.67–0.77
56141	00035720021	1970	1729	0.88	139.87 ± 0.01	0.48–0.52

2 DATA AND ANALYSIS

Swift observatory was launched in 2004 November (Gehrels et al. 2004), consisting of three sets of instruments: (1) Burst Alert Telescope (BAT), operating in the energy range of 15–150 keV (Barthelmy et al. 2005); (2) X-ray Telescope (XRT), operating in the range of 0.2–10 keV (Burrows et al. 2007); and (3) Ultraviolet and Optical Telescope (UVOT), having UV and optical coverage of 170–600 nm (Roming et al. 2005). XRT and UVOT are two narrow-field instruments, co-aligned and pointed to the centre of field of view (FOV) of BAT.

BAT is a coded aperture instrument with CdZnTe detector, having an FOV $100^{\circ} \times 60^{\circ}$ and a detection sensitivity of 5.3 mCrab (Krimm et al. 2013). XRT is a focusing telescope which employs an X-ray CCD detector with a Wolter 1 mirror set of 3.5 m focal length, with 23.6 × 23.6 arcmin FOV. The imaging array consists of 600 × 600 image pixels, each with 40 μm× 40 μm size and 2.5 arcsec pixel^{-1} resolution. It operates on three read-out modes namely imaging (IM), windowed timing (WT) and photon counting (PC) mode with few sub-modes. In IM mode, image of the object is obtained by CCD read-out. Photons are allowed to pile up and photon recognition is not done in this mode. WT mode produces 1.7 ms resolution timing with 1D position information and full energy resolution for flux less than 600 mCrab. PC mode contributes to full imaging and spectroscopic resolution with time resolution of 2.6 s.

We have analysed 33 separate *Swift*-XRT observations of IGR J18027−2016 from MJD 54141 to 56171. We have also used ∼10.5 years of *Swift*-BAT light curve to make an accurate estimation of the orbital period of this system.[1] Minimum exposure time amongst 33 *Swift*-XRT observations is ∼300 s and maximum exposure time is ∼10 ks. We used PC mode data, because 32 observations out of 33 had only this data mode. We filtered level 1 data with the task XRTPIPELINE and obtained cleaned event files for all observations. For the barycentre correction of the time column of the event files, we used the FTOOL BARYCORR. We extracted the source photons from a region with 60 arcsec radius centring the source and the background photons from a similar region in the

[1] (Krimm et al. 2013)

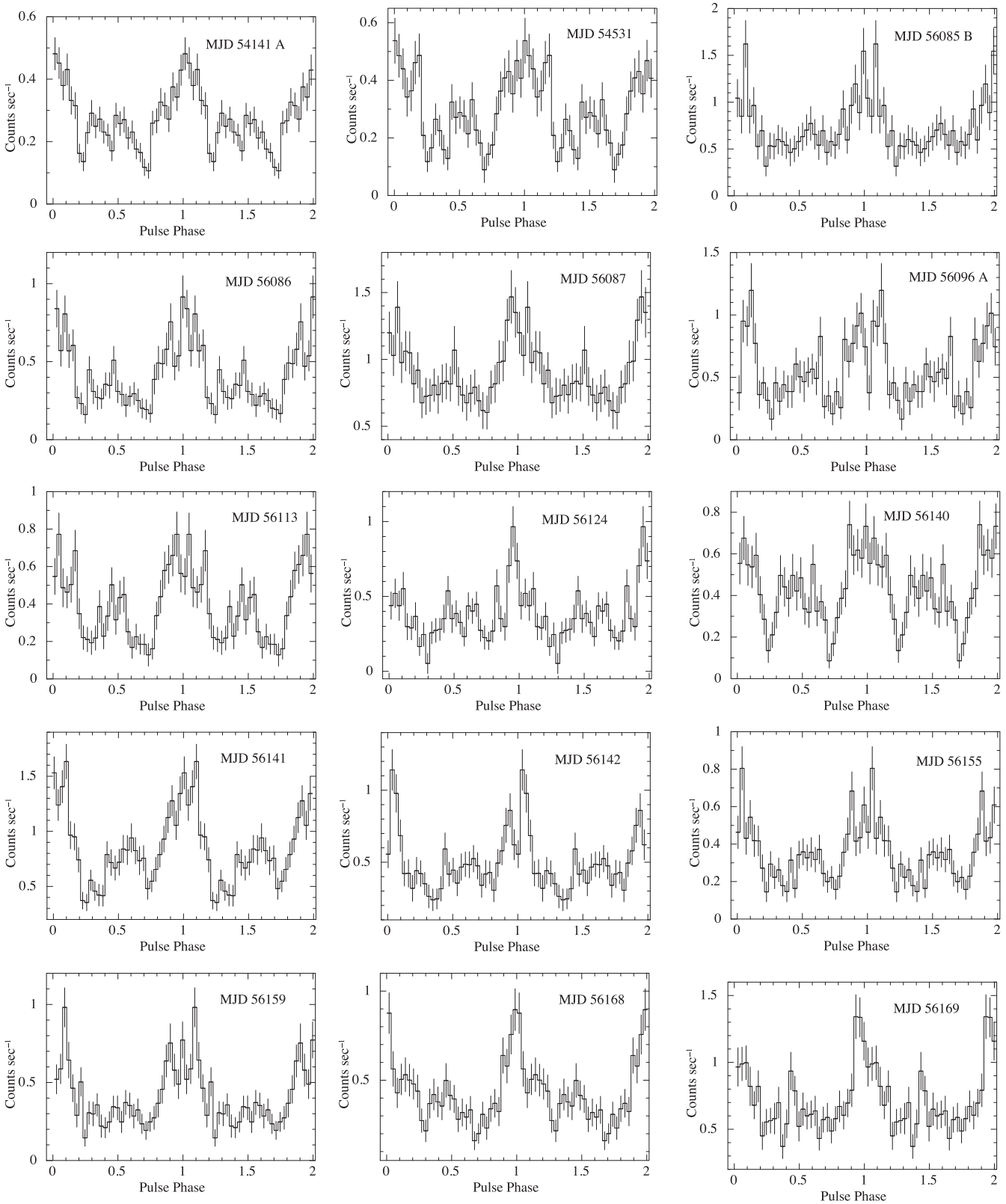

Figure 1. Pulse profiles of 15 observations with clear detection of pulsation, folded with their estimated pulse periods and with 32 phase bins per period. Main peaks of all the profiles have been aligned at phase 1.0. The MJD of each observation is labelled inside each panel.

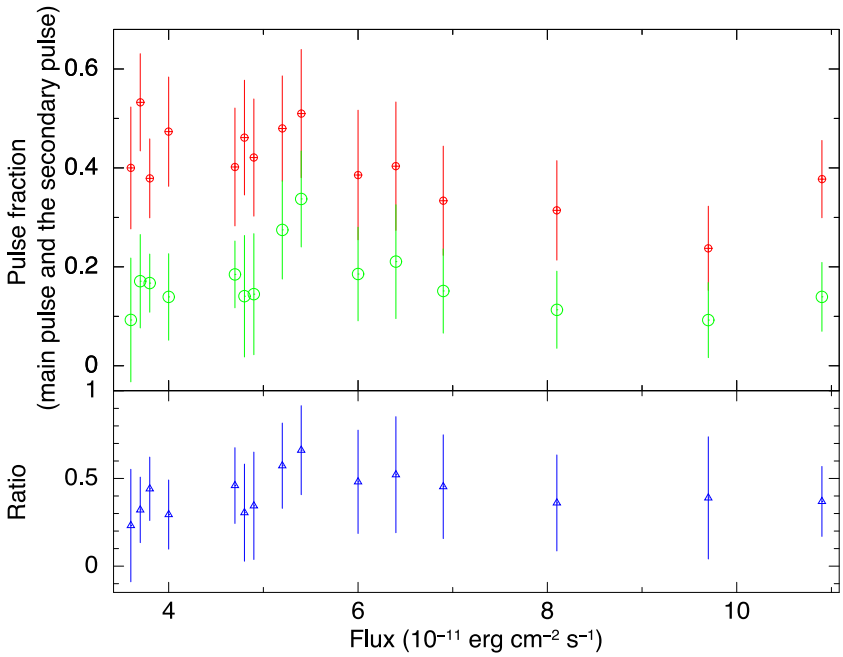

Figure 2. Top panel: pulse fraction of the main or primary (red) and secondary pulse (green) plotted as a function of flux. Bottom panel: ratio of the pulse fraction of the primary to the secondary pulse fraction plotted as a function of flux.

FOV that is free of any other X-ray sources. We used these source and background region files to extract corresponding light curves and spectra using XSELECT v2.4C.

We have generated exposure maps with the task XRTEXPOMAP to correct for the loss of flux due to some hot CCD pixels. We then used this exposure map to create ancillary file with the routine XRTMKARF which was then used for the spectral fitting in XSPEC. We obtained the response file from the latest *Swift* calibration data set CALDB v1.3.0. For five observations, the source could not be distinctly identified from the background, even with the task XRTCENTROID. For these observations, we extracted the light curves and spectra with region files centred at the RA ($18^{h}\ 02^{m}\ 41\overset{s}{.}94$) and Dec. ($-20^{\circ}\ 17'\ 17\overset{''}{.}3$) of the source (Torrejón et al. 2010). Observation at MJD 54141 was longer in duration (∼10 ks), and observations at MJD 56085 and 56096 showed significant difference in the count rate at the beginning and end of the observation. So we divided light curves and spectra of these three observations into two parts to investigate them separately. Therefore, we have total 36 separate light curves and spectra to carry out timing and spectral analysis.

2.1 Pulsation analysis

We searched for pulsations with the FTOOL task EFSEARCH for all the observations in which the source is clearly visible in the image, and the total number of source photons was more than 600. EFSEARCH results of all these light curves gave a maximum χ^2 of greater than 100 for 32 phase bins per period indicating a clear detection of the X-ray pulses. Table 1 shows the exposure time, total number of photons in 60 arcsec source region, average count rate, pulse period and orbital phase of all observations, along with the observations which were divided into two parts mentioned in Section 2, arranged in the ascending order of the total number of source photons.

Light curves of each observation with pulsation detected were folded with corresponding pulse periods. Folded pulse profiles of the 15 observations with pulsation detected are shown in Fig. 1. The pulse profiles have been aligned such that the phase of the main peak of each profile lies at 1.0. As seen in Fig. 1, most of the pulse profiles show a double-peaked structure, with a possible indication of variation in relative intensity of the peaks. Only for the purpose of comparing the strengths of the two peaks, we fitted each of these pulse profiles with two Gaussians, one for the primary pulse and the other for the secondary along with an unpulsed component. We define pulse fraction of the two peaks as the fractional area of the two Gaussians. We obtained pulse fraction for both the peaks and plotted them in the top panel of Fig. 2 along with their ratio, i.e. the relative pulse fraction of the secondary to the primary in the bottom panel as a function of flux. We see that while the overall pulse fraction has a weak negative correlation with the flux, the relative pulse fraction of the two peaks is nearly constant.

2.2 Orbital period analysis

We have searched for orbital period in the *Swift*-BAT light curve with the FTOOL task EFSEARCH and found it to be 394 843 s (4.57 d; similar to $P_{\rm orb}$ determined by Hill et al. 2005; Jain et al. 2009). We then folded the *Swift*-BAT light curve with this orbital period, and in the folded profile (shown in the top panel of Fig. 3), we can see an eclipse for duration of nearly 1/4th of the orbital period. In the bottom panel of Fig. 3, we have plotted the orbital phase-wise X-ray count rates obtained from all *Swift*-XRT light curves in three colours: pulsation detected where source photon is greater than 600 – blue; source photon less than 600 – black; faint, i.e. where source could not be seen clearly – red. To investigate any intensity variations other than the long-term averaged orbital intensity modulation, multiple observations with *Swift*-XRT during the same orbital phase range are not averaged here, unlike the orbital profile shown in fig. 3 in Bozzo et al. (2015).

In Fig. 3, the bottom panel shows the variability in count rate of the source in the orbital intensity profile with the pointed

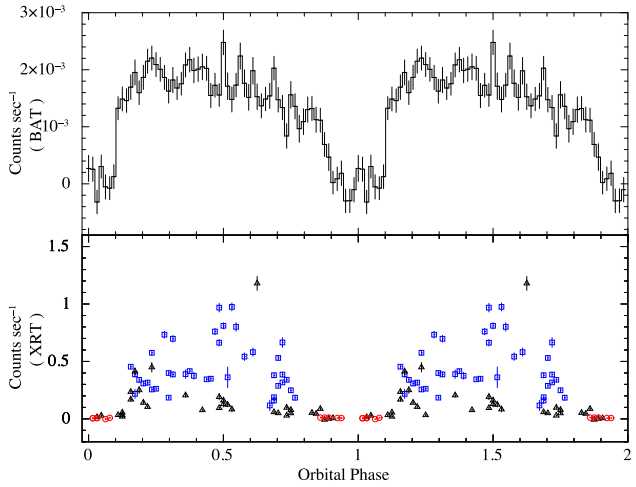

Figure 3. Top panel: orbital intensity profile of IGR J18027−2016 obtained by folding *Swift*-BAT light curve with orbital period of 394 843 s. Bottom panel: *Swift*-XRT light curves modulo same orbital period in three colours: pulsation detected where the number of source photons is greater than 600 – blue, number of source photons is less than 600 – black; faint – red.

Swift-XRT observations, whereas the *Swift*-BAT orbital intensity profile is averaged over many orbital cycles, indicating a sub-orbital variability similar to that seen in IGR J16393−4643 (Islam et al. 2015) and OAO 1657−415 (Barnstedt et al. 2008; Pradhan et al. 2014). Around orbital phase 0.5, there are multiple *Swift*-XRT observations showing significant difference in the count rates. We have shown spectra and light curve for two parts of observations carried out in the same orbital phase ranges (0.48–0.52, 0.69–0.75) in Fig. 4. The light curve is binned with 140 s (close to the spin period of the pulsar) to avoid seeing any effect of the pulse profile-related variation in the light curve. In the top panel of Fig. 4, there are about 140 photons per bin and the variability in the light curves is clearly larger than the photon noise (represented by the 1σ error bars in each bin). The number of counts per bin in the two light curves shown in the middle panel is smaller and have correspondingly larger uncertainties. No intensity variation can be ascertained in the light curves shown in the middle panel. Spectra of these two observations are shown in the lower panel of Fig. 4 which bring out the fact that in the same orbital phase range, the X-ray intensities vary by a factor of ∼10.

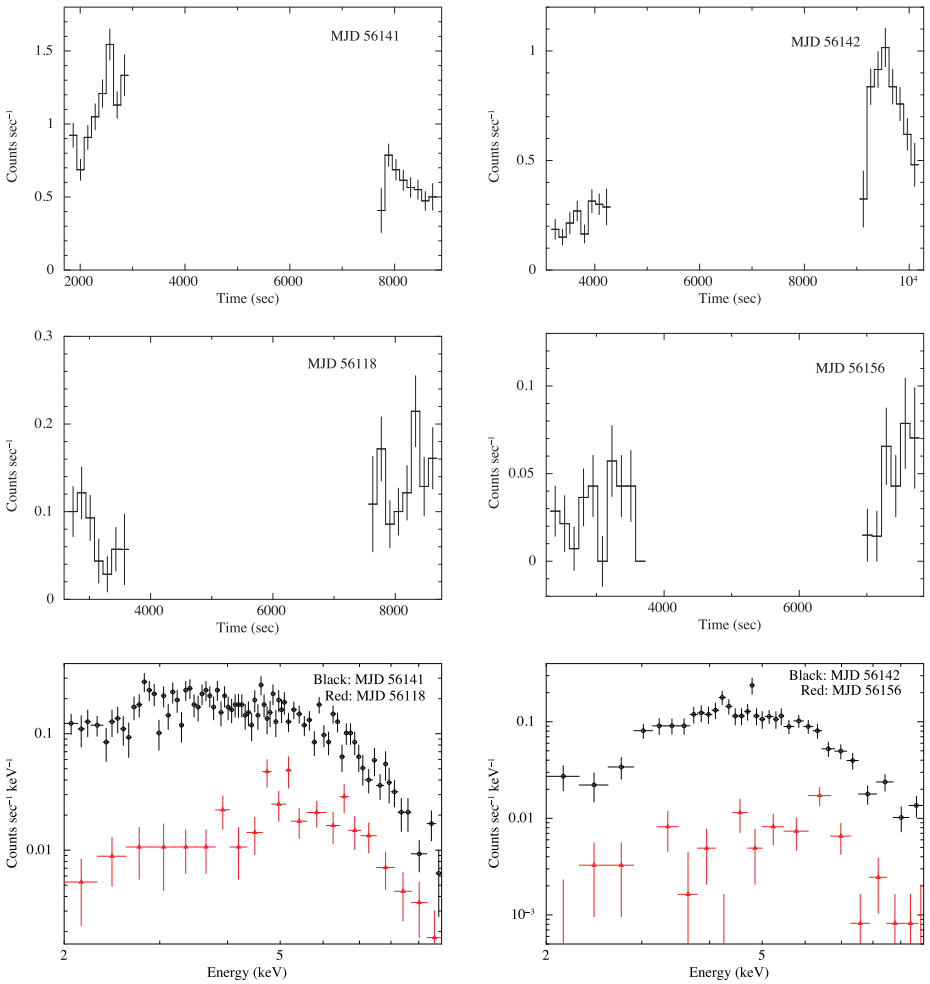

Figure 4. Left-hand panel: the top and middle panels show the light curves of two observations centred at orbital phase 0.48–0.52. In the top panel, the light curve of an observation (MJD 56141) shows a high count rate whereas the middle panel shows another observation (MJD 56118) in the same orbital phase range, having a low count rate. The lower panel is the plot of spectra of these two observations which bring out the fact that in the same orbital phase range, the X-ray intensities vary by a factor of ∼10. Right-hand panel: same is shown for another set of observations (MJD 56142 and MJD 56156) centred at orbital phase range 0.69–0.75, but showing a large change in X-ray intensities.

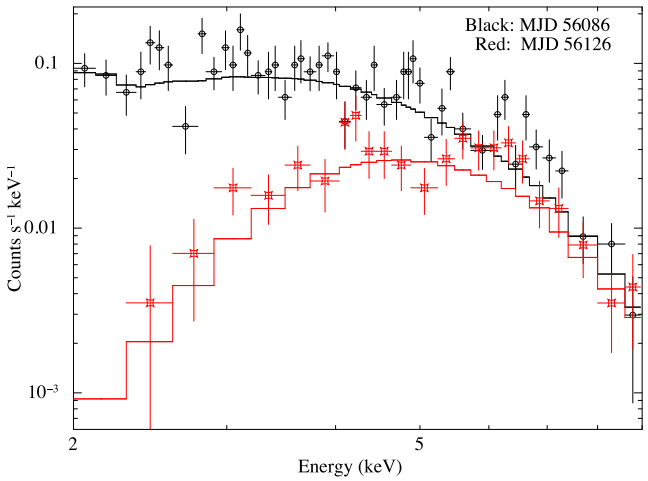

Figure 5. Spectra at MJD 56086 and 56126 are plotted together to show the variation in low-energy absorption.

2.3 Spectral analysis

We fitted X-ray spectrum for 21 observations, having moderate statistics, using XSPEC v12.8.2 in the energy range 2.0–9.0 keV. Because of limited statistics, the spectra were modelled with a power law modified by a photoelectric absorption by column density of absorbing matter along our line of sight. We have also fitted the spectra from the remaining observations only for the purpose of estimating the total flux. We have found the equivalent column density of hydrogen ($N_{\rm H}$) in the range of 10^{22}–10^{23} cm^{-2}. We have plotted two spectra in Fig. 5 obtained at MJD 56086 and 56126 to show the variation in the absorption at low energies. The spectra clearly indicate a large difference in column density. Fluxes during the out-of-eclipse orbital phase are found to be in the range of (0.4–14) $\times$ 10^{-11} erg cm^{-2} s^{-1}. We have plotted the spectral parameters $N_{\rm H}$, Γ and total flux (2.0–9.0 keV) from the system in Fig. 6.

3 DISCUSSION

In this work, we have analysed all available *Swift*-XRT observations of the HMXB source IGR J18027−2016, to study its pulsations and variability characteristics. Pulsations have been detected in all the observations having a total number of source photons greater than 600 (Table 1), and the light curves of these observations were folded with the pulse periods to create pulse profiles (Fig. 1). Some of the pulse profiles are found to have a double-peaked structure. We therefore carried out an analysis of the pulse profiles and determined the pulse fractions of the two peaks. We have plotted these pulse fractions and their ratio (primary pulse fraction to the secondary) in Fig. 2 as a function of flux and find no evidence for significant variation in the pulse profiles over a factor of ∼3 variation in flux.

The pulse profiles of accreting X-ray pulsars show strong energy dependence (Nagase 1989), usually having simpler pulse profile at higher energies (>10 keV), and complex profiles at low energies, often resulting due to phase-locked absorption. However, in a given energy band, most persistent HMXB pulsars, i.e. sources with supergiant companions, have pulse profiles that are stable over long periods of time (Vela X-1-Kreykenbohm et al. 1999, Maitra & Paul 2013). The transient pulsars, on the other hand, show very strong time/luminosity dependence of the pulse profile, which can be attributed to the changes in the structure of the X-ray emission region (accretion column) during the transient phase (Devasia et al. 2011). The limited pulse profile changes in IGR J18027−2016 are consistent with other persistent HMXBs.

The long-term averaged orbital intensity profile of this source created with *Swift*-BAT light curves is smoothly varying, having an eclipse lasting for about 1/4th of the orbit (top panel of Fig. 3). The *Swift*-XRT and *INTEGRAL* light curves, when averaged, also give smoothly varying orbital intensity profiles (Hill et al. 2005; Bozzo et al. 2015). However, the *Swift*-XRT light curves, when plotted individually for all the observations as a function of orbital phase, show a significant count rate variation outside the eclipse (bottom panel of Fig. 3). Within the same observation carried out around orbital phase 0.3–0.5 (MJD 56085), the X-ray count rates are found to vary by a factor of 36. A maximum count rate variation (a factor of 48) is shown by two non-eclipse observations at

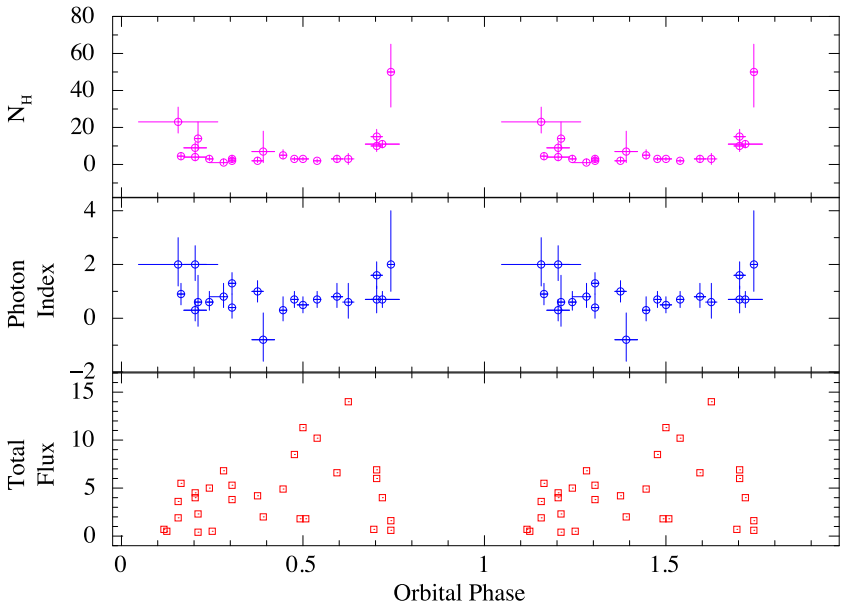

Figure 6. Variation of column density of hydrogen ($N_{\rm H}$ in units of 10^{22} cm^{-2}), photon index (Γ), total flux (F in the units of 10^{-11} erg cm^{-2} s^{-1}).

MJD 56085 and MJD 56087. These short-term variations could also be due to hydrodynamical instabilities. Manousakis & Walter (2015) have produced the hard X-ray variation observed with *INTEGRAL*-ISGRI and *RXTE* with hydrodynamical instabilities predicted by a simple model without considering intrinsic clumping or propeller effect. In some cases like in OAO 1657−415, the variations in X-ray intensity may also arise due to the accretion on to the compact object by inhomogeneous clumpy winds (Barnstedt et al. 2008; Oskinova, Feldmeier & Kretschmar 2013; Pradhan et al. 2014).

In the present work, we detect several low X-ray intensity episodes (e.g. in orbital phases 0.5 and 0.7) in the sgHMXB IGR J18027−2016, indicating these episodes to be either off-states like episodes similar to Vela X-1 (Doroshenko, Santangelo & Suleimanov 2011) or possibly the presence of clumpy wind like OAO 1657−415 (Barnstedt et al. 2008; Pradhan et al. 2014). From these XRT observations, we cannot distinguish from either of these two or other scenarios.

X-ray spectra were extracted for 21 *Swift*-XRT observations, having moderate statistics to fit with a simple power-law model, modified for photoelectric absorption. Spectra of other observations with limited statistics were also fitted with the same models just for the purpose of estimating total flux. The value of absorption column density $N_{\rm H}$ is as high as 5×10^{23} cm^{-2}, which is similar to the values obtained by Hill et al. (2005) and Walter et al. (2006), and indicates a dense circumstellar environment around the neutron star. From Fig. 6, we see an increase in $N_{\rm H}$ just before and after the eclipse, similar to that seen in 4U 1538−52 (Mukherjee et al. 2006; Rodes-Roca et al. 2015).

IGR J18027−2016 presents an interesting case of a supergiant source showing evidence of low X-ray intensity states, similar to well-known sources like Vela X-1. Detailed X-ray timing and spectroscopic observations of IGR J18027−2016 at various orbital phases with other X-ray missions would be useful to understand the nature of these low-intensity states.

ACKNOWLEDGEMENTS

We thank the referee Roland Walter for suggestions that helped us to improve the paper. The data used for this work have been obtained through the High Energy Astrophysics Science Archive (HEASARC) Online Service provided by NASA/GSFC. We have also used the public light curves from the *Swift*-BAT site.

REFERENCES

Augello G., Iaria R., Robba N. R., Di Salvo T., Burderi L., Lavagetto G., Stella L., 2003, ApJ, 596, L63
Barnstedt J. et al., 2008, A&A, 486, 293
Barthelmy S. D. et al., 2005, Space Sci. Rev., 120, 143
Bozzo E., Stella L., Ferrigno C., Giunta A., Falanga M., Campana S., Israel G., Leyder J. C., 2010, A&A, 519, A6
Bozzo E., Romano P., Ducci L., Bernardini F., Falanga M., 2015, Adv. Space Res., 55, 1255
Burrows D. N. et al., 2007, Proc. SPIE, 6686, 7
Devasia J., James M., Paul B., Indulekha K., 2011, MNRAS, 417, 348
Doroshenko V., Santangelo A., Suleimanov V., 2011, A&A, 529, A52
Doroshenko V., Santangelo A., Ducci L., Klochkov D., 2012, A&A, 548, A19
Gehrels N. et al., 2004, ApJ, 611, 1005
Göğüş E., Kreykenbohm I., Belloni T. M., 2011, A&A, 525, L6
Grebenev S. A., Lyashenko O. V., Pavlinsky M. N., Sunyaev R. A., 1999, Astrophys. Lett. Commun., 38, 89
Hill A. B. et al., 2005, A&A, 439, 255
Islam N., Maitra C., Pradhan P., Paul B., 2015, MNRAS, 446, 4148
Jain C., Paul B., Dutta A., 2009, Res. Astron. Astrophys., 9, 1303
Kreykenbohm I., Kretschmar P., Wilms J., Staubert R., Kendziorra E., Gruber D. E., Heindl W. A., Rothschild R. E., 1999, A&A, 341, 141
Krimm H. A. et al., 2013, ApJS, 209, 14
Maitra C., Paul B., 2013, ApJ, 763, 79
Manousakis A., Walter R., 2015, A&A, 575, A58
Moon D.-S., Eikenberry S. S., 2001, ApJ, 549, L225
Moon D.-S., Eikenberry S. S., Wasserman I. M., 2003, ApJ, 582, L91
Mukherjee U., Raichur H., Paul B., Naik S., Bhatt N., 2006, J. Astrophys. Astron., 27, 411
Nagase F., 1989, PASJ, 41, 1
Odaka H., Khangulyan D., Tanaka Y. T., Watanabe S., Takahashi T., Makishima K., 2013, ApJ, 767, 70
Oskinova L. M., Feldmeier A., Kretschmar P., 2013, in Zhang C. M., Belloni T., Méndez M., Zhang S. N., eds, Proc. IAU Symp. 290, Feeding Compact Objects: Accretion on All Scales. Cambridge Univ. Press, Cambridge, p. 287
Pradhan P., Maitra C., Paul B., Islam N., Paul B. C., 2014, MNRAS, 442, 2691
Reig P., 2011, Ap&SS, 332, 1
Revnivtsev M. G. et al., 2004, Astron. Lett., 30, 382
Rodes-Roca J. J., Mihara T., Nakahira S., Torrejón J. M., Giménez-García Á., Bernabéu G., 2015, A&A, 580, A140
Roming P. W. A. et al., 2005, Space Sci. Rev., 120, 95
Sguera V. et al., 2005, A&A, 444, 221
Sidoli L., Romano P., Mereghetti S., Paizis A., Vercellone S., Mangano V., Götz D., 2007, A&A, 476, 1307
Torrejón J. M., Negueruela I., Smith D. M., Harrison T. E., 2010, A&A, 510, A61
Walter R. et al., 2006, A&A, 453, 133
Walter R., Lutovinov A. A., Bozzo E., Tsygankov S. S., 2015, A&AR, 23, 2

This paper has been typeset from a TEX/LATEX file prepared by the author.